



Research on the flexural behavior of polypropylene fiber reinforced concrete beams with hybrid reinforcement of GFRP and steel bars

Bingyan Wei · Xiongjun He · Weiwei Wu ·
Chao Wu · Jia He

Received: 16 August 2023 / Accepted: 22 March 2024
© The Author(s) 2024

Abstract To study the flexural behavior of glass fiber (GFRP) bars and steel bars hybrid reinforced polypropylene fiber concrete (Hybrid-PFRC) beams, one GFRP-PFRC beam, one Steel-PFRC beam, and five Hybrid-PFRC beams were designed and fabricated. The effects of the different area ratio (A_f/A_s) of GFRP to steel bars and polypropylene fiber (PP) volume fraction on the flexural behavior of Hybrid-PFRC beams were investigated through experiments.

The research results indicated that the Hybrid-PFRC beams' load–deflection curves exhibited trilinear characteristics with specimen cracking and steel bars yielding as turning points. As A_f/A_s increased, the flexural bearing capacity of Hybrid-PFRC beams increased, the deflection decreased, the crack spacing and width decreased, and the ductility decreased. The addition of PP did not significantly improve the flexural bearing capacity and cracking moment of Hybrid-PFRC beams, but it greatly enhanced the ductility of the beam. Moreover, PP had good advantages in controlling crack propagation in the beam. The article also used the theoretical model to predict and analyze the flexural behavior of Hybrid-PFRC beams. When predicting the maximum crack width of Hybrid-PFRC beams, when PP is not added to the beam, the bonding coefficient k_b should be greater than 1.4; When PP is added to the beam, it is recommended that the bonding coefficient k_b should not exceed 1.4.

B. Wei · X. He · W. Wu · C. Wu
School of Transportation and Logistics Engineering,
Wuhan University of Technology, Wuhan 430063, China
e-mail: weibingyan@whut.edu.cn

X. He
e-mail: hxjwhut@163.com

W. Wu
e-mail: www92@whut.edu.cn

C. Wu
e-mail: chaowu@whut.edu.cn

B. Wei · X. He · W. Wu · C. Wu
Hubei Province Highway Engineering Research Center,
Wuhan 430063, China

W. Wu
School of Engineering, The University of British
Columbia, Kelowna, BC V1V 1V7, Canada

J. He (✉)
Department of the Built Environment, Eindhoven
University of Technology, PO Box 513,
5600 MB Eindhoven, the Netherlands
e-mail: j.he@tue.nl

Keywords Hybrid reinforced beams · GFRP bar ·
Flexural behavior · Crack propagation · PP · Ductility

1 Introduction

Since the introduction of reinforced concrete structures (RC), they have long been the preferred structural design form in civil engineering and have been widely used. However, from the actual engineering



use situation, the durability of RC has always been plagued by steel bar corrosion, and steel bar corrosion is the leading cause of RC failure [1, 2]. Therefore, Fiber-reinforced polymer (FRP) bars with high tensile strength, good corrosion resistance, and lightweight can be used instead of steel bars [3]. However, FRP bars have a low elastic modulus and no yield stage, resulting in low stiffness, large crack width, and low ductility of FRP reinforced concrete (FRP-RC) beams. FRP-RC beams show prominent brittle failure characteristics, which do not align with the ductility design concept of concrete structures [4, 5]. To solve the above problems, a hybrid reinforcement using steel and FRP bars is an efficient and workable option. This arrangement method can use the advantages of high tensile strength and good corrosion resistance of FRP bars and the benefits of high stiffness and good ductility of steel bars, which can solve the structural durability problem caused by corrosion of steel bars and overcome the disadvantages of poor performance of FRP-RC, which is an ideal form of reinforcement [6–10].

However, there is a significant difference in the performance of FRP and steel bars, resulting in the flexural behavior of Hybrid-RC beams being different from Steel-RC beams and FRP-RC beams. Consequently, researchers have researched and analyzed the flexural behavior of Hybrid-RC beams to promote the broad application of Hybrid-RC beams in structural engineering. Ge et al. [11] reported that the deflection, average crack spacing, and ductility coefficient of Hybrid (BFRP and steel)-RC beams were between Steel-RC and BFRP-RC beams under the same load. Thamrin et al. [12] showed that the flexural bearing capacity of Hybrid-RC beams was higher than that of ordinary Steel-RC beams, and the higher the ratio (A_f/A_s) of FRP bars area to steel bars area, the greater the bearing capacity of the beam, and the lower the ductility and flexural stiffness values of the beam. Pang et al. [13] pointed out that A_f/A_s had a significant impact on the ductility of Hybrid-RC beams, and it was necessary to control A_f/A_s reasonably to ensure that the Hybrid-RC beams' ductility satisfies the standards. Numerous studies also confirmed this conclusion [14–17]. Bui et al. [18, 19] concluded that parameters such as hybrid reinforcement ratio, concrete's compressive strength, arrangement of tensile bars, and length of FRP bars significantly influenced the structural behavior of

Hybrid-RC beams. Hussein et al. [20] stated that the FRP bars' bond performance determined the flexural load capacity and post-yield stiffness of the Hybrid-RC beams.

Although the Hybrid-RC beams have good flexural behavior, it should be noted here that the maximum crack width and deflection of Hybrid-RC beams were much larger than those of Steel-RC beams under normal service conditions, and these unfavorable conditions limited the promotion and application of Hybrid-RC beams [21]. Improving the concrete strength and crack resistance is an effective method to promote the flexural behavior of Hybrid-RC beams, such as using fiber-reinforced concrete, which has been used in several studies in recent years [22–24].

Moreover, Polypropylene fibers (PP) have excellent characteristics such as low density, low price, easy dispersion, and chemical stability, and they have broad engineering application prospects. Adding PP to concrete enhances the flexural strength, splitting tensile strength, compressive strength, and flexural toughness of concrete, improving concrete's corrosion, fire, and abrasion resistance [25, 26]. PP can effectively enhance the load-bearing capacity of concrete after cracking. Therefore, in this study, the key to conducting flexural toughness tests on PFRC is determining PP's volume fraction. In addition, there have been more studies on the flexural behavior of Steel-PFRC beams and FRP-PFRC beams in published studies, while there has been less research on the flexural behavior of Hybrid-PFRC beams. Therefore, the influence of PP volume fraction on the flexural bearing capacity, deflection, crack propagation, and ductility of Hybrid-PFRC beams was studied, and a theoretical model was used to predict the flexural behavior of Hybrid-PFRC beams.

2 Test program

2.1 Materials

2.1.1 GFRP and steel bars

This study used HRB400 hot-rolled ribbed steel bars as the beam's tensile longitudinal bars and HPB300 grade plain round steel bars as the beam's compression and stirrup bars. The mechanical characteristics test results of the GFRP bars and HRB400 steel



bars are displayed in Table 1. It should be noted that the mechanical performance parameters of GFRP bars and steel bars were sourced from the material supplier.

2.2 Polypropylene fiber (PP)

This article selected 12 mm long bundle-shaped monofilament polypropylene short fiber produced by Hunan Changsha Huixiang Fiber Company, with a diameter of 32.7 μm , a density of 0.91 g/cm^3 , an elastic modulus of 4.24 GPa, a tensile strength of 469 MPa, and an elongation of 28.4%.

2.3 Concrete

The design strength grade of the concrete in this paper was C55, and the concrete's water-cement ratio (W/B) was 0.30. The cement was Hefeng Huaxin Cement Company's (Hubei, China) P-O42.5 regular Portland cement; the fine aggregate was 0~4.75 mm mechanism sand produced by Hefeng self-built sand and gravel plant, the coarse aggregate was 5~20 mm continuously graded gravel produced by Hefeng self-built sand and gravel plant, the fly ash was F class I fly ash produced by Huaneng Jingmen Thermal Power Co., Ltd., the mineral powder was Yichang Tengkuo S95 grade mineral powder, the water was domestic tap water. The water-reducing agent was ART-JS polycarboxylate acid, a high-performance water-reducing agent produced by Tianjin Jin Xinyuan Technology Development Co., Ltd.(Tianjin, China). Its concrete

mix ratio is shown in Table 2, and a standard concrete cube with a side length of 150 mm was made. According to the GB/T 50081–2019 design guide [27], the compressive strength f_{cu} of the concrete cube was measured as shown in Table 2. It should be noted that the PP volume fraction used for the bending performance test of Hybrid-PFRC beams is 0.2 and 0.4%, so Table 2 only provides f_{cu} with plain concrete, PP volume fraction of 0.2% and PP volume fraction of 0.4%.

2.4 Determination of PP volume fraction

2.4.1 PFRC workability test

Table 2 shows that the concrete mix ratio was used to design PFRC. A total of 7 groups of PFRC were designed here, with different PP volume fractions of 0, 0.1%, 0.2%, 0.3%, 0.4%, 0.5%, and 0.7%, corresponding to PP masses of 0, 0.9 kg, 1.8 kg, 2.7 kg, 3.6 kg, 4.5 kg, and 6.3 kg. The PFRC was tested in each group according to JG/T 248–2009 and GB/T 50080–2016 design guidelines [28, 29], and the PFRC workability test was measured. According to PFRC and workability tests, it can be concluded that when the volume fraction of PP is between 0 and 0.4%, the slump, flowability, water-retention, and cohesiveness of concrete is better; When the volume fraction of PP is between 0.5 and 0.7%, the slump, flowability, water-retention, and cohesiveness of concrete is general.

Table 1 GFRP and HRB400 steel bars mechanical characteristics






Bars	Diameter (mm)	Elasticity modulus (GPa)	Yield strength (MPa)	Ultimate strength (MPa)
GFRP	 8	45.66	–	910.00
	 12	45.42	–	869.56
	 16	45.08	–	855.68
HPB300 steel bars	 8	195.5	450.00	515.00
HRB400 steel bars	 12	206.05	521.20	642.00

Table 2 Concrete' mix ratio and f_{cr} (Unit: kg/m³)

Group	Cement	Coal ash	Mineral powder	Fine aggregate	Coarse aggregate	Water	Water reducer	PP fiber	f_{cr} (MPa)	f_{cr-avg} (MPa)
NC-1									69.15	
NC-2	400	40	70	677	1104	153	5.61	0	71.15	70.31
NC-3									70.63	
PP-0.2%-1									72.63	
PP-0.2%-2	400	40	70	677	1104	153	5.61	1.8	71.49	72.46
PP-0.2%-3									73.26	
PP-0.4%-1									74.5	
PP-0.4%-2	400	40	70	677	1104	153	5.61	3.6	73.63	74.43
PP-0.4%-3									75.16	

NC is plain concrete; PP-0.2% represents a PP volume fraction of 0.2%; PP-0.4% represents a PP volume fraction of 0.4%; and f_{cr-avg} represents the average value of f_{cr} .

2.5 PFRC bending toughness test

The PFRC specimens of 100 mm × 100 mm × 400 mm were made, three specimens were prepared for each group, and the four-point bending toughness test was carried out for the PFRC specimens according to the CECS13: 2009 design guide [30] after 28d of curing, and the test loading device are shown in Fig. 1a, b, c shows the PFRC specimen's load–deflection curves. The study analyzed the flexural strength f_u and flexural toughness index I of the PFRC specimens, which the f_u was calculated by using Eq. (1), and the I was calculated by using Eq. (2) [30, 31]. The estimated average flexural strength and average flexural toughness index of each group of PFRC are shown in Fig. 1d.

$$f_u = \frac{FL}{bh^2} \quad (1)$$

where f_u =the flexural strength of the PFRC specimen (MPa); F =bending load (N); L =span length of PFRC specimen (This article is 300 mm); b =the specimen's width (This article is 100 mm); h =the specimen's height (This article is 100 mm).

$$I = \frac{S_1}{S_0} \quad (2)$$

where S_0 =the area enclosed by the horizontal coordinate δ and the coordinate axis of the point (the initial crack point) where the load–deflection curve of the test-collected specimen changes from linear to non-linear; and S_1 =the area enclosed by the coordinate axis when the horizontal coordinate is 10δ .

It can be seen from Fig. 1 that as the PP volume fraction increases, the toughness and flexural strength of concrete specimens can be improved to different degrees, among which the flexural behavior of the specimens is the most excellent when the PP volume fraction is 0.4%. The flexural toughness index of the specimens is better when the PP volume fraction is 0.7%. When the PP volume fraction is less than 0.2%, the specimen load–displacement curves do not have prominent falling segments and the specimen instantly fractures; On the contrary, there is a significant falling segment. In addition, as the PP volume fraction exceeds 0.4%, the flexural strength of the specimen has a downward trend. Moreover, because PP is a flexible fiber, when the volume



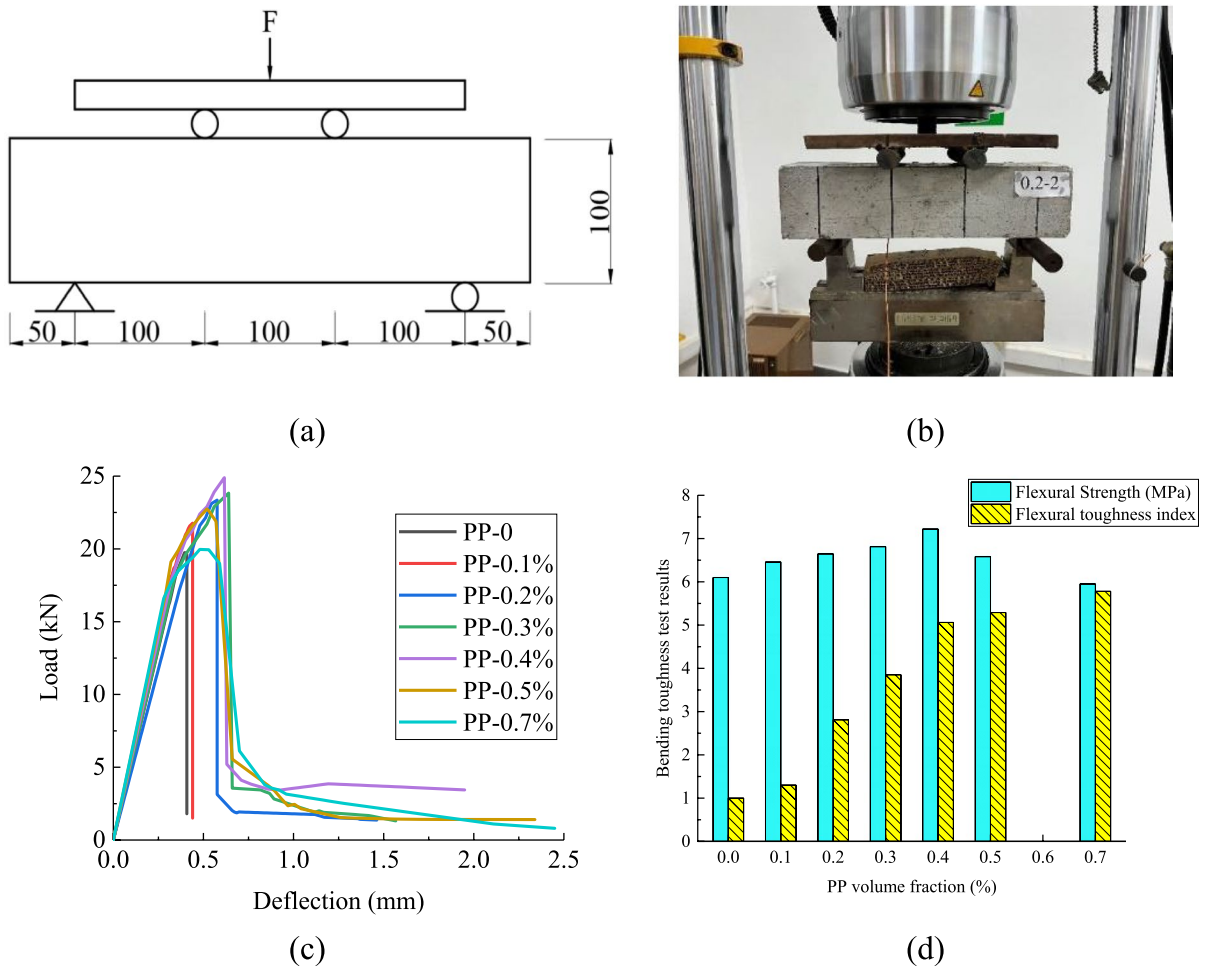


Fig. 1 PFRC bending toughness test: **a** schematic diagram; **b** actual loading device; **c** load–deflection curves of PFRC; and **d** test results

fraction of PP is large, the corresponding decrease in the load–deflection curve of PFRC specimens is relatively gentle, indicating that PP can improve the toughness of concrete to a certain extent and absorb strong impact energy for failure. Especially when the volume fraction of PP is greater than 0.2%, the toughness index of PFRC specimens significantly increases with the increase of PP volume fraction. However, an excessive volume fraction of PP can reduce the flexural strength of PFRC specimens. Analyzing the reason, PP does not form a dense and integral spatial network structure in the concrete matrix but generates numerous weak interfaces, reducing its strength. Therefore, based on the results of the bending toughness test, the PP volume fraction was selected as 0,

0.2%, and 0.4% to study the influence of PP on the flexural behavior of Hybrid-PFRC beams.

2.6 Specimens design

A total of seven rectangular cross-section beams with sizes of 110 mm × 180 mm × 1200 mm were fabricated for this test (shown in Fig. 2a), and all the test beams were cross-sectioned with double-layer reinforcement (shown in Fig. 2b). In addition, the thickness of the concrete cover was 20 mm.

In this test, the Steel-RC beam was designed as a balance-reinforced beam, while the GFRP-RC beam was designed as a super-reinforced beam according to ACI 440.1R-15 [32]. Hybrid-RC beams refer to the

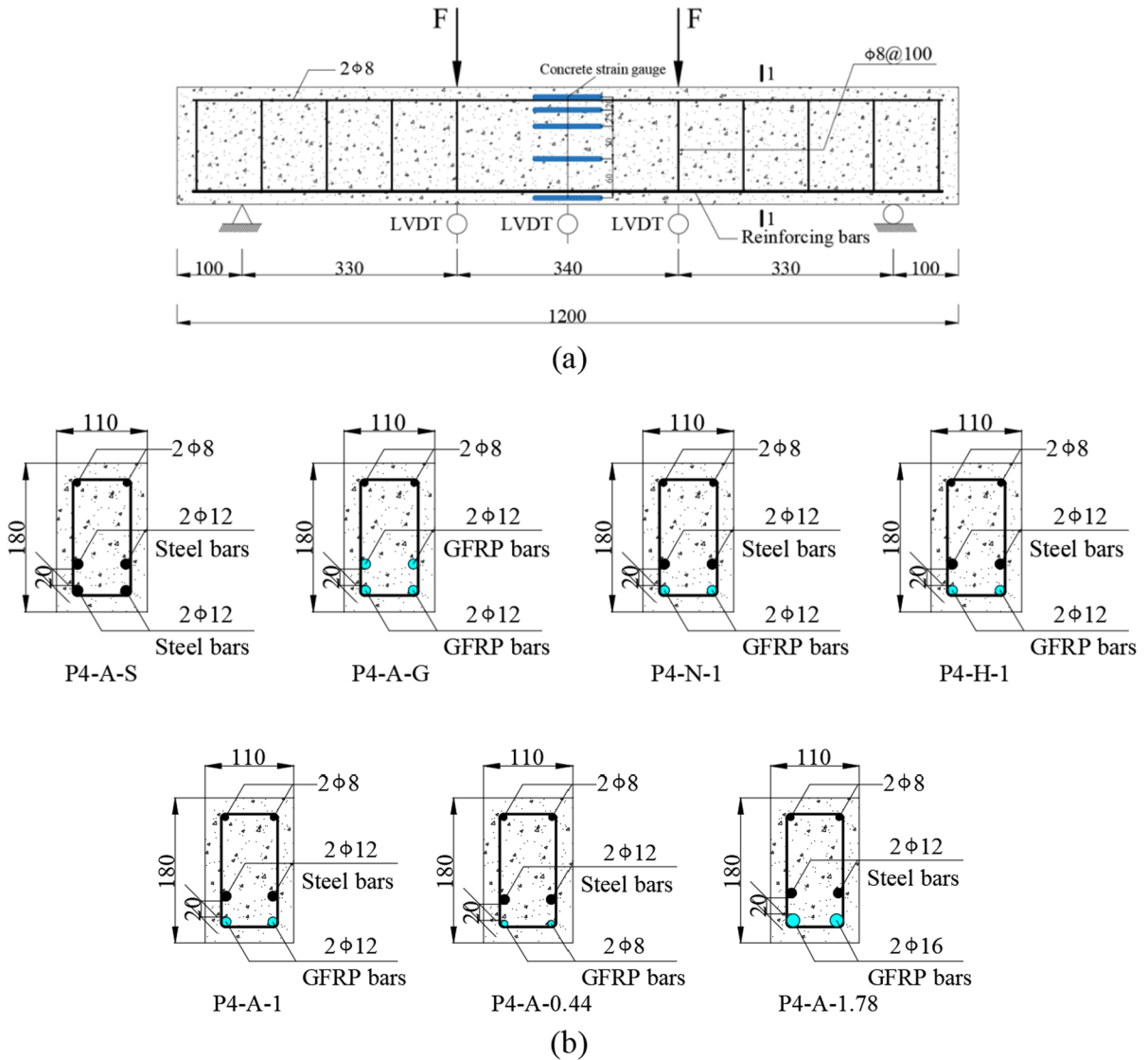


Fig. 2 Test beams (Unit: mm): **a** beam size details; and **b** 1–1 cross-section reinforced

principle of “equal strength replacement” and define two hybrid reinforcement ratios $\rho_{sf,s}$ and $\rho_{sf,f}$, which can be expressed as Eq. (3) and Eq. (4). To ensure that the Hybrid-RC beam is a balance-reinforced failure, the hybrid reinforcement ratio should satisfy Eq. (5) and Eq. (6) [13, 15]. The detailed parameters of the test beam are shown in Table 3.

$$\rho_{sf,s} = \frac{E_s A_s + E_f A_f}{E_s b d} = \rho_s + \frac{E_f}{E_s} \rho_f \quad (3)$$

$$\rho_{sf,f} = \frac{f_y A_s + f_{fd} A_f}{f_{fd} b d} = \rho_s \frac{f_y}{f_{fd}} + \rho_f \quad (4)$$

$$\rho_{sf,s} \leq 0.64 \beta_1 \frac{f'_c}{f_y} \frac{E_s \epsilon_{cu}}{E_s \epsilon_{cu} + f_y} \quad (5)$$

$$\rho_{sf,f} \geq 1.19 \beta_1 \frac{f'_c}{f_{fd}} \frac{E_f \epsilon_{cu}}{E_f \epsilon_{cu} + f_{fd}} \quad (6)$$



Table 3 Details of tested beams

Beam	$A_f(\text{mm}^2)$	$A_s(\text{mm}^2)$	$\rho_{sf,s}(\%)$	$\rho_{sf,f}(\%)$	$f_c'(\text{MPa})$	PP volume fraction (%)	Failure mode
P4-A-S	–	452.39	3.12	–	59.54	0.4	SY-CC
P4-A-G	452.39	–	–	3.12	59.54	0.4	CC
P4-N-1	226.19	226.19	2.08	2.91	56.25	0	SY-CC
P4-H-1	226.19	226.19	2.08	2.91	57.97	0.2	SY-CC
P4-A-1	226.19	226.19	2.08	2.91	59.54	0.4	SY-CC
P4-A-0.44	100.53	226.19	1.85	2.01	59.54	0.4	SY-CC
P4-A-1.78	402.13	226.19	2.38	4.10	59.54	0.4	SY-CC

0.44, 1, and 1.78 represent the A_f/A_s ; Steel yielding and concrete crushing is SY-CC, and CC refers to concrete crushing.

where E_s =steel bars' elastic modulus (MPa); E_f =GFRP bars' elastic modulus (MPa); A_s =area of steel bars (mm^2); and A_f =area of GFRP bars (mm^2); $\rho_f = A_f/(bd)$ =GFRP bars ratio; b =width (mm) and d =effective height of beam cross-section (mm); $\rho_s = A_s/(bd)$ =steel bars ratio; f_y =yield stress in steel bars (MPa); f_{fd} =design tensile stress in GFRP bars (MPa) ($f_{fd} = 0.7f_{fu}$, where f_{fu} =the GFRP bars' maximum tensile strength) [32]; f_c' =the concrete's cylinder compressive strength (MPa) ($f_c' = 0.8f_{cu}$) [33]; ϵ_{cu} =concrete's ultimate compressive strain, and it is 0.003; ϵ_y =steel yield strain; β_1 =the ratio of the neutral axis depth to the depth of the comparable rectangular concrete stress block, β_1 is taken according to ACI 440.1R-06 [34] and β_1 can be estimated by Eq. (7), but β_1 cannot be less than 0.65.

$$\beta_1 = 0.85 - \frac{0.05(f_c' - 28)}{7} \quad (7)$$

2.7 Test device

The loading of the test beam is shown in Fig. 3. To verify the plane section assumption, concrete strain gauges of the type BFH120-80AA-R1-P300 were glued in the span of the test beam to measure the concrete strain. To measure the strain of the steel bars and GFRP bars, strain gauges of the type BFH120-3AA were glued in the span of the bottom longitudinal bars. The loading device was controlled by a hydraulic servo-control system with a bearing capacity of 5000 kN. A 300 kN force sensor was used to record load values at different loading times. The test beams were loaded with graded monotonic loading according to the GB/T 50152–2012 design guide [35]. During the loading process, a crack width

measuring instrument (as shown in Fig. 3c) was used to record the crack width, and load values, deflection, and concrete strain of the beams under different loads were recorded until the test beams were damaged.

3 Experimental results and analysis

3.1 Strain analysis

Figure 4 shows the strain distribution of concrete in typical test beams under different loads. It can be seen from Fig. 4 that the strain at each point of the concrete in the pure bending section is approximately proportional to the distance from that point to the neutral axis, and the strain at the mid-span section of the test beam along the beam height is in good agreement with the assumption of a flat section.

3.2 Cracking moment

The cracking moment of Hybrid-RC beams is mainly related to the moment of inertia of the beam cross-section and the concrete strength. ACI 440.1R-15 design guide [32] uses Eq. (8) to calculate the cracking moment of the FRP-RC beam. In addition, the CSA-S806-12 design guide [36] uses Eq. (9) to calculate the cracking moment of the FRP-RC beam.

$$M_{cr} = \frac{0.62\lambda\sqrt{f_c'}I_g}{y_t} \quad (8)$$

$$M_{cr} = \frac{0.6\lambda\sqrt{f_c'}I_g}{y_t} \quad (9)$$

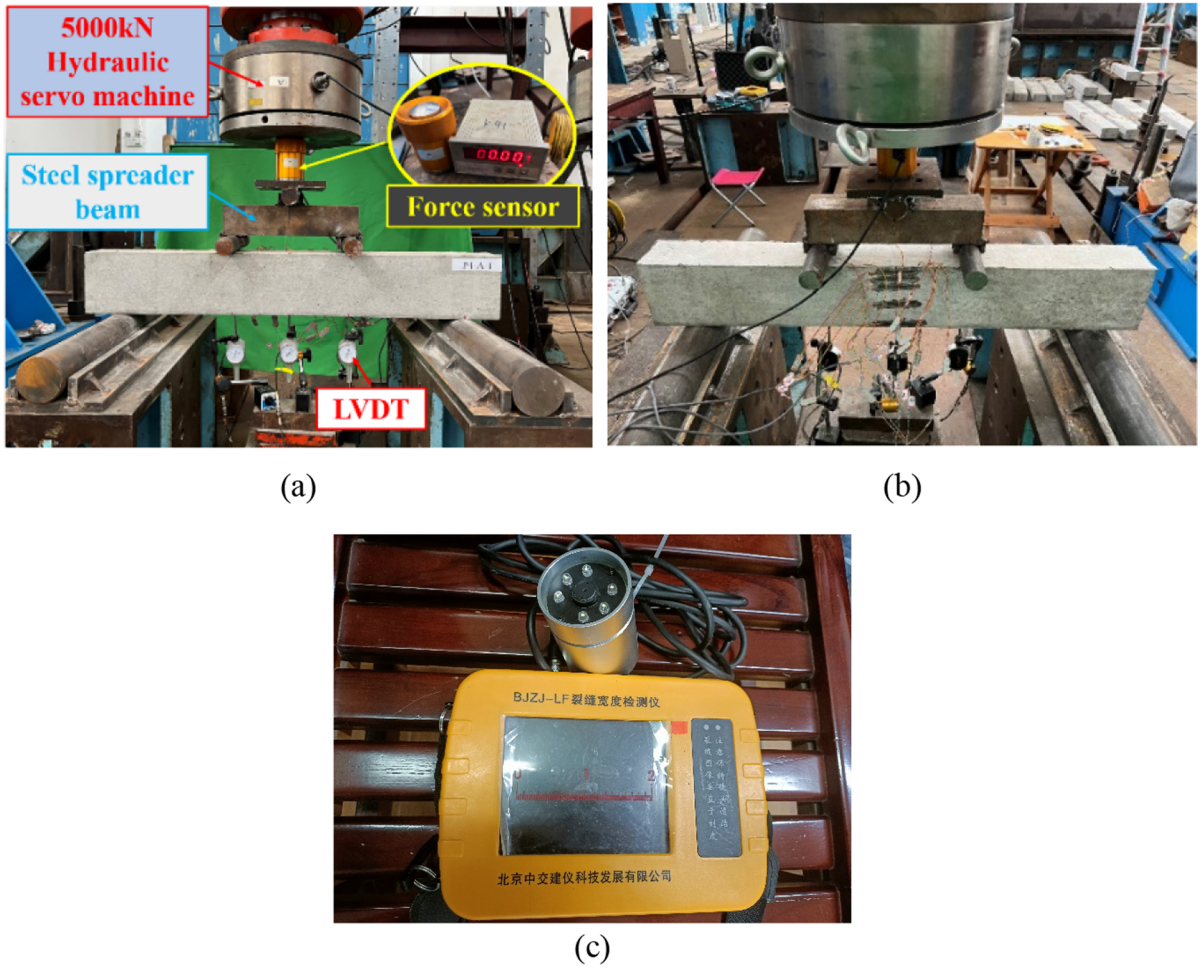


Fig. 3 Test setup: a front; b opposite; and c crack width measuring instrument

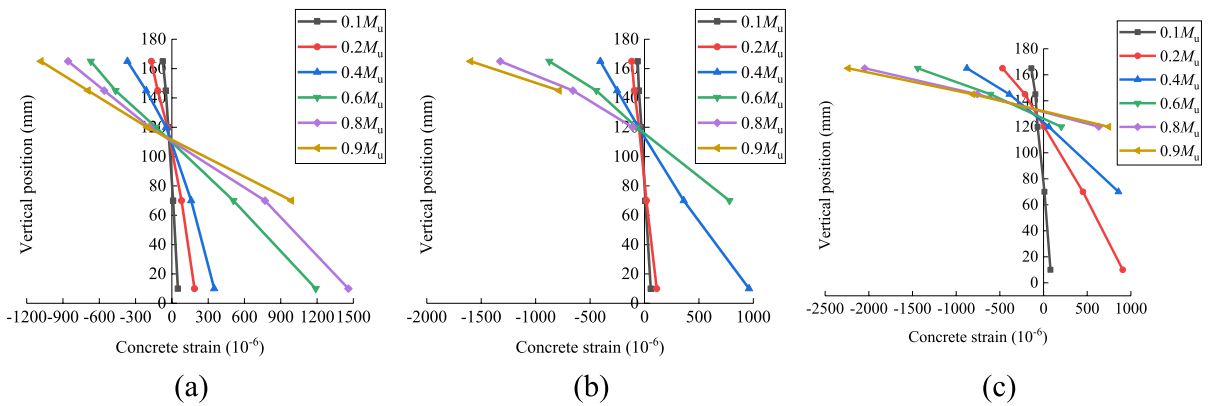


Fig. 4 Strain distribution of concrete in test beams: a P4-A-S; b P4-A-G; and c P4-A-1



where I_g = the beam cross-section's moment of inertia; and $I_g = bh^3/12$, where h = the beam cross-section's height; λ = modification factor that considers the lighter concrete's diminished mechanical capabilities and $\lambda = 1$ in this research; y_t represents the distance from the centroid axis of the gross section.

Table 4 provides the experimental and theoretical values of the cracking moment of the test beam. It can be seen from Table 4 that for the Hybrid-PFRC beam, when the PP volume fraction increases from 0 to 0.2% and 0.4%, the cracking moment of the Hybrid-PFRC beam rises by 2.4 and 7.6%, respectively. With the increase of A_f/A_y , the cracking moment of the Hybrid-PFRC beam shows a decreasing trend. In addition, the predicted cracking moment value calculated by the ACI 440.1R-15 model [32] and the CSA-S806-12 model [36] is in good agreement with the tested results and both smaller than the experimental value, which is conservative, indicating that using two theoretical models to predict the Hybrid-PFRC beams' cracking moment is appropriate.

3.3 Ultimate moment

Qu et al. [6] used the equivalent rectangular stress graph and the cross-section internal force balance to provide the stress (f_f) calculation formula for FRP bars in the ultimate state of Hybrid-RC beams (as shown in Eq. (10)) and the ultimate bending moment (M_u) calculation formula for beams (as shown in Eq. (11)).

$$f_f = \sqrt{\frac{1}{4} \left(\frac{A_s f_y}{A_f} + E_f \epsilon_{cu} \right)^2 + \left(0.85 \frac{\beta_1 f_c'}{\rho_f} - \frac{A_s f_y}{A_f} \right) E_f \epsilon_{cu}} - \frac{1}{2} \left(\frac{A_s f_y}{A_f} + E_f \epsilon_{cu} \right) \leq f_{fu} \quad (10)$$

$$M_u = (\rho_f f_f + \rho_s f_y) \left(1 - 0.59 \frac{\rho_f f_f + \rho_s f_y}{f_c'} \right) b d^2 \quad (11)$$

In addition, Ge et al. [11] simplified the material constitutive model and used an equivalent rectangular stress diagram to replace the concrete curve stress in the compression zone, providing a formula for calculating the ultimate bending moment of the Hybrid-RC beam, as shown in Eq. (12).

$$M_u = \alpha_1 f_c b d^2 \xi \left(1 - \frac{\xi}{2} \right) \quad (12)$$

where f_c = concrete prisms' axial compressive strength, and $f_c = 0.76 f_{cu}$ [37]; ξ = the height of the relative compression zone of the cross-section, and ξ can be estimated by Eq. (13).

$$\xi = \frac{f_y \rho_s - \epsilon_{cu} E_f \rho_f + \sqrt{(f_y \rho_s - \epsilon_{cu} E_f \rho_f)^2 + 4 \alpha_1 \beta_1 \epsilon_{cu} E_f \rho_f f_c}}{2 \alpha_1 f_c} \quad (13)$$

where $\epsilon_{cu} = 0.0033$; α_1 and β_1 parameter meaning refer to GB 50010–2010 [37] when the concrete strength level is less than C50, $\alpha_1 = 1.0$, $\beta_1 = 0.8$; when the concrete strength level is more than C80, $\alpha_1 = 0.94$, $\beta_1 = 0.74$; and when the concrete strength is between C50 and C80, the linear interpolation method can be used to take values.

Table 4 Flexural mechanical results of test beams

Beam	PP volume fraction (%)	M_{cr-exp} (kN · m)	$M_{cr-ACI Eq.(8)}$ (kN · m)	$\frac{M_{cr-ACI Eq.(8)}}{M_{cr-exp}}$	$M_{cr-CSA Eq.(9)}$ (kN · m)	$\frac{M_{cr-CSA Eq.(9)}}{M_{cr-exp}}$
P4-A-S	0.4	3.30	2.84	0.86	2.75	0.83
P4-A-G	0.4	2.97	2.84	0.96	2.75	0.93
P4-N-1	0	3.30	2.76	0.84	2.67	0.81
P4-H-1	0.2	3.38	2.80	0.83	2.71	0.80
P4-A-1	0.4	3.55	2.84	0.80	2.75	0.77
P4-A-0.44	0.4	3.63	2.84	0.78	2.75	0.76
P4-A-1.78	0.4	2.64	2.84	1.08	2.75	1.04
Average value				0.88		0.85
Standard deviation				0.10		0.09
Coefficient of variation (%)				11.4		11.8

Table 5 Comparison between theoretical and test values of the ultimate moment

Beam	PP volume fraction (%)	M_{u-exp} (kN · m)	M_{u-Qu} Eq.(11) (kN · m)	$\frac{M_{u-Qu} \text{ Eq.(11)}}{M_{u-exp}}$	M_{u-Ge} Eq.(12) (kN · m)	$\frac{M_{u-Ge} \text{ Eq.(12)}}{M_{u-exp}}$
P4-A-S	0.4	26.28	24.89	0.95	25.21	0.96
P4-A-G	0.4	29.37	26.4	0.90	27.16	0.92
P4-N-1	0	26.4	21.21	0.80	22.63	0.86
P4-H-1	0.2	27.39	21.53	0.79	22.92	0.84
P4-A-1	0.4	28.22	21.72	0.77	23.18	0.82
P4-A-0.44	0.4	23.1	19.75	0.85	20.67	0.89
P4-A-1.78	0.4	30.2	23.38	0.77	25.16	0.83
Average value				0.83		0.88
Standard deviation				0.06		0.05
Coefficient of variation (%)				8		6

Table 5 provides the experimental and theoretical value of the ultimate bending moment of the test beam. It can be seen from Table 5 that when the PP volume fraction and reinforcement area are the same, the ultimate bending moment of the P4-A-S beam is the smallest, the P4-A-G beam is the largest, and the ultimate bending moment of the P4-A-1 beam is between the two. In addition, for Hybrid-PFRC beams, the PP volume fraction and A_f/A_s have a significant impact on the beam's ultimate bending moment, and the beams' ultimate bending moment can be increased either by increasing the PP volume fraction or by increasing the A_f/A_s .

It can be seen from Table 5 that the experimental value of the ultimate bending moment is in good agreement with the theoretical value obtained from the calculations of Eq. (11) and Eq. (12), and the prediction accuracy of Eq. (12) proposed by Ge et al. [11] is better. In addition, the theoretical value calculated by Eq. (11) and Eq. (12) is smaller than the experimental value, indicating that using Eq. (11) or Eq. (12) to calculate the ultimate moment of Hybrid-PFRC beams is reasonable.

3.4 Moment-deflection curves and prediction

Figure 5 shows the bending moment mid-span deflection curves of all test beams. It can be seen from Fig. 5a that when the PP volume fraction and reinforcement ratio are the same, under the same load, the deflection and ultimate bending moment of the P4-A-S beam is the smallest, the deflection and ultimate bending moment of P4-A-G beam is the largest. The deflection and ultimate bending moment of

the P4-A-1 beam are between the two. It can be seen from Fig. 5b that when the reinforcement ratio is the same, the effect of the PP volume fraction on the flexural behavior of Hybrid-PFRC beams is noticeable. The deflection of Hybrid-PFRC beams gradually decreases, and the ultimate bending moment gradually increases when the PP volume fraction gradually increases from 0 to 0.2% and 0.4%. Figure 5c shows that this significantly impacts the flexural behavior of Hybrid-PFRC beams. When the PP volume fraction and load are the same, the P4-A-1.78 beam has the minor deflection and maximum moment, the P4-A-0.44 beam has the largest deflection and minimum moment, and the P4-A-1 beam has a deflection and moment between the two.

For the Hybrid-RC beam, the deflection generated by the Hybrid-RC beam under load should be predicted and verified. For steel bars before yielding, the ACI 440.1R-15 design guide [32] predicts the deflection of FRP-RC beams based on the effective moment of inertia method proposed by Bischoff et al. [38] (as shown in Eq. (14)). After the steel bars yield, Yoon et al. [39] proposed a method to calculate the effective moment of inertia of the steel bars after yielding based on the research results of Bischoff et al. [40], as shown in Eq. (15). However, more relevant studies are needed to test the accuracy of the model of Yoon et al.

$$I_e = \frac{I_{cr}}{1 - \gamma \left(\frac{M_{cr}}{M_a} \right)^2 \left(1 - \frac{I_{cr}}{I_g} \right)} \leq I_g \quad (14)$$



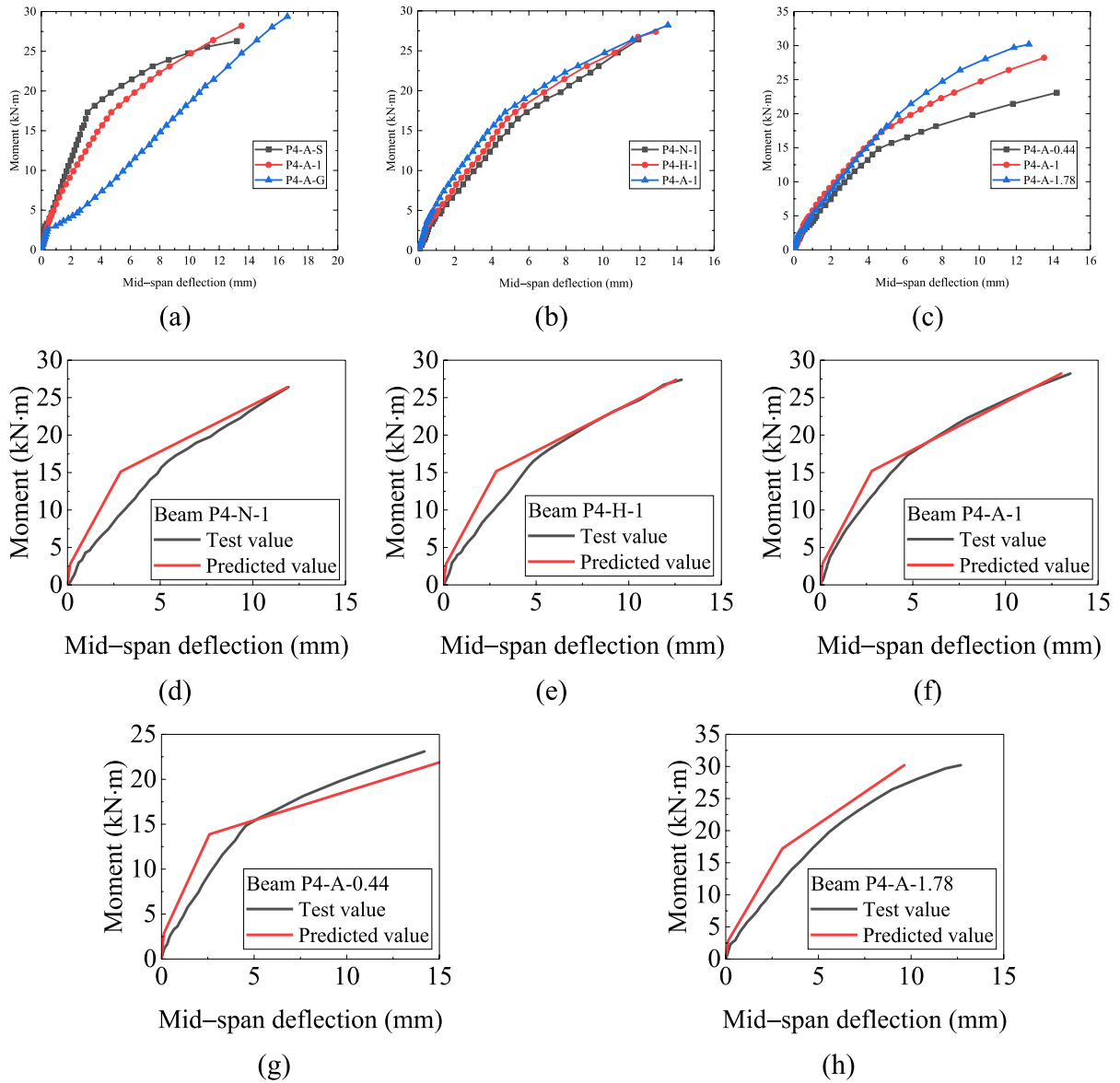


Fig. 5 Load–deflection relationships for test beams: **a** three kinds of beams; **b** different PP volume fraction; **c** different A_f/A_s ; **d** P4-N-1; **e** P4-H-1; **f** P4-A-1; **g** P4-A-0.44; and **h** P4-A-1.78

where I_e =effective moment of inertia; I_{cr} =moment of inertia of the cracked section, and $I_{cr} = bd^3k^3/3 + (n_sA_s + n_fA_f)d^2(1-k)^2$,
 $k = \sqrt{2(n_f\rho_f + n_s\rho_s) + (n_f\rho_f + n_s\rho_s)^2} - (n_f\rho_f + n_s\rho_s)$,

where $n_s = E_s/E_c$, $n_f = E_f/E_c$, and E_c =elastic modulus of concrete [41]; γ =the parameter that changes the stiffness of the beam along its length direction, $\gamma = 1.72 - 0.72M_{cr}/M_a$, where M_{cr} =cracking moment, and M_a =applied moment.

$$I_{e2} = \frac{I_{cr}}{\frac{I_{cr}}{I_y} + \left(\frac{M_y}{M_a}\right)\left(1 - \frac{I_{cr}}{I_y}\right) - \gamma\left(\frac{M_{cr}}{M_a}\right)^2\left(1 - \frac{I_{cr}}{I_g}\right)} \quad (15)$$

where M_y =yield moment; and I_y =rotational moment of inertia when steel bars yield.

Based on the above, the effective moment of inertia of the Hybrid-RC beams before and after the steel bars yield was obtained using the ACI 440.1R-15 model [32] and

the Yoon et al. [39] model. Then, the mid-span deflection of the Hybrid-RC beams was predicted and analyzed using Eq. (16), as shown in Fig. 5d–h. Figure 5d–h shows that when the Hybrid-PFRC beam is not cracked, the predicted mid-span deflection of the beam is smaller than the test value, and the predicted curve slope is greater than the test curve slope; When the beam is between the cracking and yielding stages, the predicted deflection at the mid-span of the beam is significantly smaller than the test value, and the slope of the predicted moment-deflection curve is significantly greater than the slope of the test moment-deflection curve; After the beam yielding, the predicted deflection at the mid-span of the beam is closer to the test value, and the corresponding curve slope is also closer. Therefore, using theoretical models to predict the mid-span deflection of Hybrid-PFRC beams during the loading stage is reasonable.

$$\Delta_m = \frac{Pa(3L^2 - 4a^2)}{48E_c I_e} \quad (16)$$

where P = service load; a = the beam's shear span, and L = the beam's span.

3.5 Crack distribution and failure mode

Figure 6 displays the final crack morphology of all test beams. Figure 6 shows that all test beams mostly exhibit vertical cracks in the pure bending zone and oblique cracks in the bending shear area. In addition, the failure mode of the Hybrid-PFRC beam and

Steel-PFRC beam was steel bars yielding, concrete in the compression zone being crushed, and the GFRP bars inside the Hybrid-PFRC beam did not fracture, consistent with the failure mode designed in Table 3. The failure mode of the GFRP-PFRC beam was a shear failure, which is inconsistent with the failure mode designed in Table 3, mainly manifested as an oblique crack penetrating the bending shear area. Analyzing the reasons, the ultimate bearing capacity and deformation of the GFRP-PFRC beam is relatively large, while the number of stirrups is relatively small, which may lead to shear failure of the GFRP-PFRC beam. In addition, comparing the failure mode of test beams P4-N-1, P4-H-1, and P4-A-1, it can be seen that the change in PP volume fraction has little effect on the failure mode of the beam. Through comparison, it was found that at the same reinforcement ratio, the number of cracks in GFRP-PFRC beam P4-A-G was relatively small, and the crack spacing was rather large. The number of cracks in Steel-PFRC beam P4-A-S was pretty large, and the spacing was small, while the number of cracks and spacing in the Hybrid-PFRC beam were between the two. For Hybrid-PFRC beams, as the PP volume fraction increases, the number of cracks in the beam gradually increases, and the crack spacing decreases. In addition, as A_f/A_s increases, the number of cracks in the Hybrid-PFRC beam gradually increases, and the crack spacing gradually decreases.

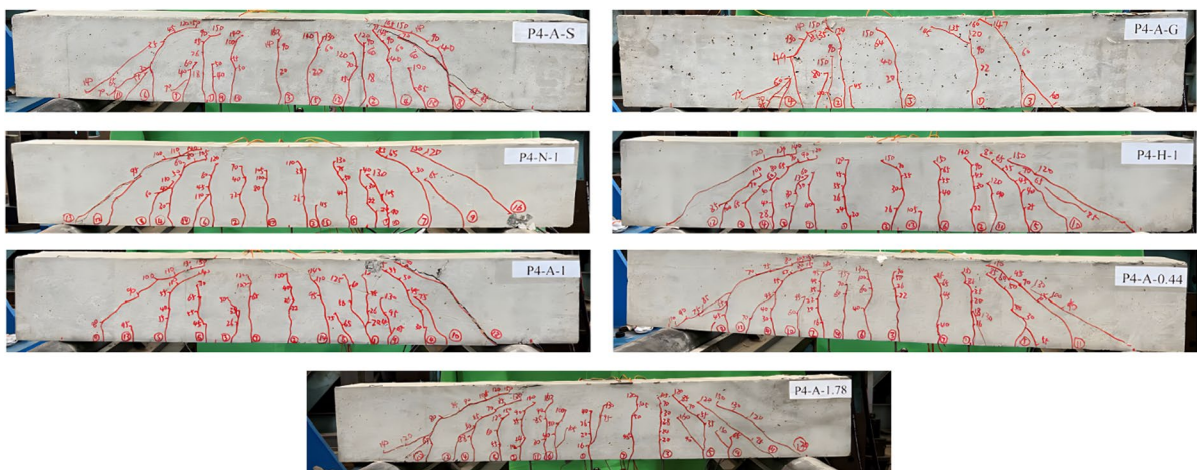


Fig. 6 Cracking patterns at failure



3.6 Crack width and spacing

The moment-maximum crack width and average crack spacing of the test beams are shown in Fig. 7. During the test, when the test beam cracks, record the width of each crack according to the graded loading, and finally, select the crack with the largest width to draw the curve. In addition, when two cracks appear in the test beam, the distance between the two cracks needs to be measured. When the third crack appears, measure the distance between the crack closest to it, and so on, until the test beam fails. Finally, calculate the average crack spacing and draw a curve. As known from Fig. 7a, at the same reinforcement ratio, the crack width of Steel-PFRC beam P4-A-S is the smallest, the crack width of GFRP-PFRC beam P4-A-G is the largest, and the crack width of Hybrid-PFRC beam P4-A-1 is in between. As can be seen from Fig. 7b, for Hybrid-PFRC beams, the crack width of Hybrid-PFRC beams decreases significantly when the PP volume fraction gradually increases, thus indicating that the addition of PP enhances the crack resistance of the beams and strengthens the toughness of concrete beams. In addition, after the cracking of the Hybrid-PFRC beam, due to the PP bridging effect, the crack width of the Hybrid-PFRC beam is reduced under service load conditions, and the risk of corrosion of the tensile steel bars inside the beam is reduced. Of course, PP cannot significantly reduce the crack width of Hybrid-PFRC beams. When the service load exceeds 60% of the ultimate load, the maximum crack width of Hybrid-PFRC beams exceeds 0.5 mm, while under the same conditions, the maximum crack width of Steel-PFRC beam is only 0.25 mm, which limits the application of Hybrid-PFRC beams in practical engineering. In addition, it can be seen from Fig. 7c that the crack width of Hybrid-PFRC beams decreases gradually with increasing A_f/A_s . It can be seen from Fig. 7d that the average crack spacing of Steel-PFRC beams is the smallest, the GFRP-PFRC beam is the largest, and Hybrid-PFRC beams are between when the PP volume fraction and bending moments are the same. For the Hybrid-PFRC beams, when the PP volume fraction increases from 0 to 0.4%, the average crack spacing gradually decreases, indicating that the addition of PP inhibits crack propagation.

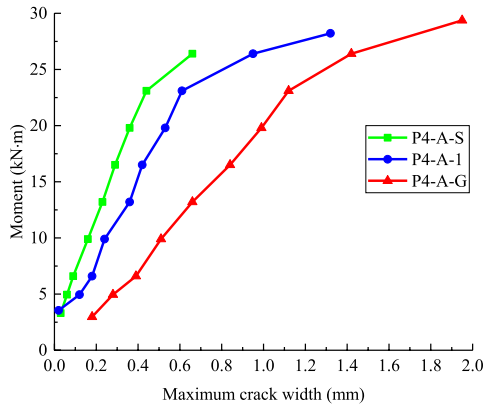
In addition, the average crack spacing of Hybrid-PFRC beams decreases with the increase of A_f/A_s .

For FRP-RC beams, to predict the maximum crack width of the beams, the ACI 440.1R-06 design guide [34] and CSA S806-12 design guide [36] use Eq. (17) to calculate the FRP-RC beams' maximum crack width.

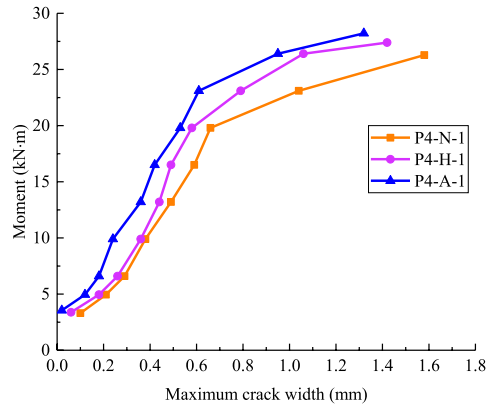
$$w_{\max} = 2\varepsilon_f \beta k_b \sqrt{d_c^2 + \left(\frac{s}{2}\right)^2} \quad (17)$$

where w_{\max} = the maximum crack width; ε_f = tensile strain at the center of the tensile bars, $\varepsilon_f = M_a / (A_f E_f + A_s E_s) d \left(1 - \frac{k}{3}\right)$, where $k = \sqrt{2(n_f \rho_f + n_s \rho_s) + (n_f \rho_f + n_s \rho_s)^2} - (n_f \rho_f + n_s \rho_s)$; β = the ratio of the neutral axis's distance from the tensile surface to that of the centroid of the tensile zone, and $\beta = (h - kd) / [d(1 - k)]$; d_c = thickness of cover from tension face to center of the closest bar; s = longitudinal tensile bars spacing; k_b = the bond coefficient, the bonding coefficient $k_b = 1.0$ between steel bars and concrete, and the bond coefficient $k_b = 1.4$ between FRP bars and concrete [34].

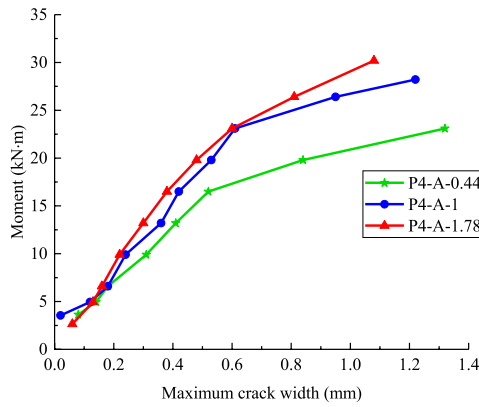
Figure 7e–i gives the comparative analysis of the experimental and predicted values of maximum crack width for Hybrid-PFRC beams. Figure 7e–i shows that before the yield of the test beam, the predicted maximum crack width is relatively close to the test value, while after the yield of the test beam, the predicted maximum crack width has a large error with the test value. In addition, Fig. 7e indicates that when there is no PP inside the Hybrid-RC beam, the predicted maximum crack width is closer to the test value when $k_b > 1.4$; And Fig. 7f–i shows that when PP is added to the Hybrid-RC beam, the predicted maximum crack width is close to the test value when $k_b \leq 1.4$. Analyzing the reasons, adding PP reduced the crack width of Hybrid-RC beams, while Eq. (17) is not considering the volume fraction of PP, and increasing in k_b resulted in an increase in the predicted maximum crack width. Therefore, when predicting the maximum crack width of Hybrid-PFRC beams, it is recommended that $k_b > 1.4$ when the PP volume fraction is 0; When the volume fraction of PP is not 0, it is recommended that $k_b \leq 1.4$.



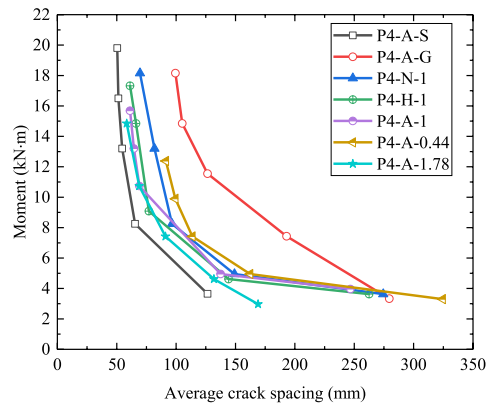
(a)



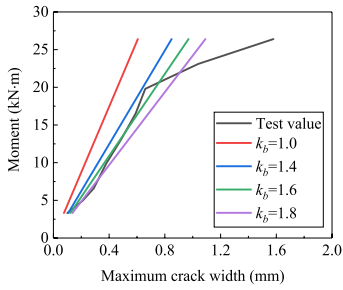
(b)



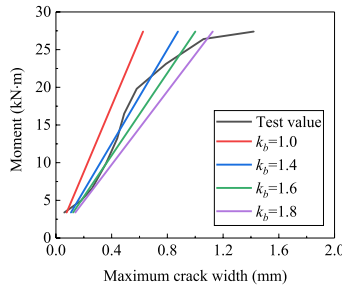
(c)



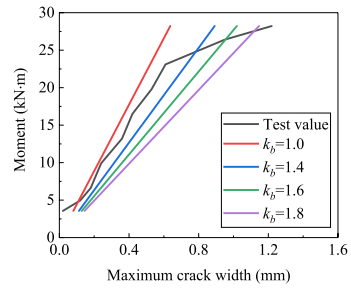
(d)



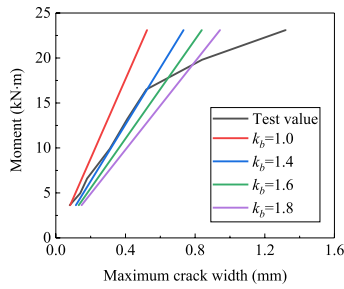
(e)



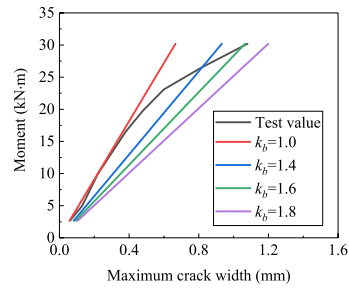
(f)



(g)



(h)



(i)



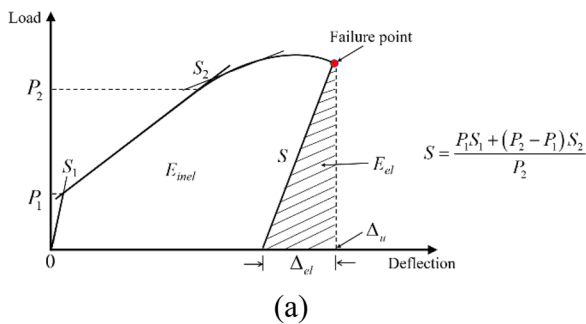
◀**Fig. 7** Test results: **a** maximum crack width of three types of reinforced beams; **b** maximum crack width of different PP volume fractions; **c** maximum crack width of different A_f/A_s ; **d** average crack spacing of test beams; **e** relationship between the test and predicted values of beam P4-N-1; (f) relationship between test and predicted values of beam P4-H-1; (g) relationship between test and predicted values of beam P4-A-1; (h) relationship between test and predicted values of beam P4-A-0.44; and (i) relationship between test and predicted values of beam P4-A-1.78

3.7 Ductility

3.7.1 Deformation index

CSA S6-10 design guide [42] and Jaeger et al. [43] proposed to evaluate the ductility performance of FRP-RC structures by using a deformation index based on the deformation capacity of beams, and the deformation index is calculated as shown in Eq. (18).

$$\mu_{\Delta} = \frac{\varphi_u}{\varphi_{0.001}} \frac{M_u}{M_{0.001}} \quad (18)$$



where φ_u and M_u are the ultimate curvature and ultimate bending moment, respectively; and $\varphi_{0.001}$ and $M_{0.001}$ represent the curvature and bending moment of the concrete in the compression zone when the strain is 0.001.

3.8 Energy ductility index

Naaman and Jeong [44] showed that the ductility of a structure can be determined by the ratio of the total energy to the elastic energy at the time of destructive loading, and the calculation of the ductility index based on the energy method is shown in Eq. (19).

$$\mu_E = 0.5 \left(\frac{E_T}{E_{el}} + 1 \right) \quad (19)$$

where $E_T (= E_{inel} + E_{el})$ is the total energy, E_{inel} represents plastic energy, E_{el} represents elastic energy, E_{inel} and E_{el} can be calculated according to Fig. 8a.

However, the load–deflection curve of the actual Hybrid-RC beam is shown in Fig. 8b, which is delineated by the cracking point, steel yield point, and

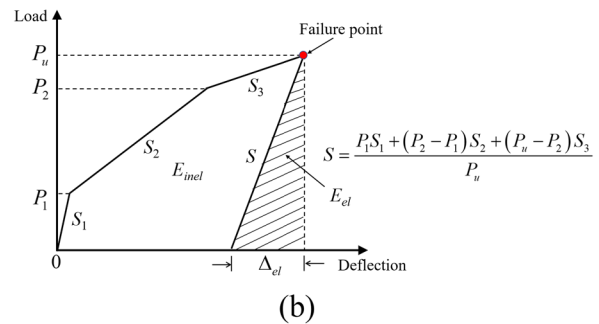


Fig. 8 E_{inel} and E_{el} calculation methods: **a** Naaman and Jeong [44]; and literature [45]

Table 6 Ductility value of test beams

Beam	PP volume fraction (%)	φ_u ($10^{-5}/\text{mm}$)	M_u (kN · m)	$\varphi_{0.001}$ ($10^{-6}/\text{mm}$)	$M_{0.001}$ (kN · m)	μ_{Δ}	E_T (kN · m)	E_{el} (kN · m)	μ_E
P4-A-S	0.4	1.27	26.28	5.57	11.55	5.18	1.59	0.51	2.05
P4-A-G	0.4	1.42	29.37	7.16	14.85	3.91	1.54	1.43	1.04
P4-N-1	0	1.27	26.4	6.2	12.87	4.21	1.13	0.84	1.17
P4-H-1	0.2	1.32	27.39	6.36	13.2	4.31	1.32	0.84	1.29
P4-A-1	0.4	1.36	28.23	6.36	13.2	4.57	1.51	0.82	1.42
P4-A-0.44	0.4	1.11	23.1	4.93	10.23	5.09	1.33	0.66	1.51
P4-A-1.78	0.4	1.46	30.2	7.16	14.85	4.14	1.42	0.94	1.26

ultimate failure point. Therefore, E_{inel} and E_{el} use be calculated according to Fig. 8b.

Table 6 shows the ductility index of the test beams. It can be seen from Table 6 that the ductility index μ_{Δ} calculated using Eq. (18) is greater than 4 for all the test beams except for the P4-A-G beam, which satisfies the requirement that the ductility index of beams with rectangular cross-section should not be less than 4 [42, 43]. In addition, the P4-A-S beam has the best ductility, the P4-A-G beam has the worst ductility, and the Hybrid-PFRC beams have a ductility in between. As the Hybrid PFRC beam, as A_f/A_s increases, the ductility index of the Hybrid-PFRC beam gradually decreases, indicating that A_f/A_s has a significant impact on the ductility of the Hybrid-PFRC beam. Table 6 shows that the PP volume fraction has a significant effect on the ductility index of Hybrid-PFRC beams. When the PP volume fraction increases from 0 to 0.2% and 0.4%, the ductility index of the beams increases by 10.3 and 21.4%, respectively, indicating that PP can effectively improve the ductility of Hybrid-PFRC beams.

4 Conclusion

This study investigated the effects of PP volume fraction on the flexural bearing capacity, failure mode, deflection deformation, crack development, and ductility of Hybrid-PFRC beams. In addition, the theoretical model was used to predict the flexural behavior of Hybrid-PFRC beams, and the conclusions obtained are as follows:

1. When the PP volume fraction is 0.4, PFRC flexural strength is the largest; When the volume fraction of PP is 0.7%, the flexural toughness index of PFRC is the best. In addition, when the volume fraction of PP is more significant than 0.4%, the PFRC flexural strength shows a downward trend.
2. When the bending moment is the same, the flexural bearing capacity, crack width and spacing, deflection deformation, and ductility of Hybrid-PFRC beams are between Steel-PFRC and GFRP-PFRC beams.
3. When the reinforcement area is the same, the ductility of Hybrid-PFRC beams is smaller than that of Steel-PFRC beams, and the ductility index of Hybrid-PFRC beams only reaches 70–80% of Steel-PFRC beam. In addition, for Hybrid-PFRC beams, when the A_f/A_s ratio is small, the ductility of Hybrid-PFRC beams is close to that of Steel-PFRC beam.
4. As the PP volume fraction increases from 0 to 0.2% and 0.4%, the cracking moment of Hybrid-PFRC beams increases by 2.4 and 7.6%, the flexural bearing capacity increases by 3.8 and 6.9%, and the ductility index of the beams increases by 10.3 and 21.4%, respectively. In addition, the addition of PP significantly reduces the crack width and spacing of Hybrid-PFRC beams.
5. With the increase of A_f/A_s , the flexural bearing capacity of Hybrid-PFRC beams gradually increases, the crack spacing and crack width decrease, and the number of cracks increases. Still, the ductility of the beams decreases. For this reason, it is necessary to control A_f/A_s reasonably so that the ductility of the beam meets the design code requirements.
6. The predicted flexural behavior of the Hybrid-PFRC beams is in accordance with the test results. In addition, when predicting the maximum crack width of Hybrid-PFRC beams, it is recommended that $k_b > 1.4$ when the PP volume fraction is 0; When the volume fraction of PP is not 0, it is recommended that $k_b \leq 1.4$.
7. Because only one beam of each type was tested in this test, and the potential changes in the weighing of structural materials, the placement of steel bars cages, and the four-point bending test method may affect the accuracy of the test results, the test results have a certain degree of error, and more tests are needed to verify them in the future.

Funding The National Natural Science Foundation of China (No. 51178361), the China Scholarship Council (No. 202206950027), the Major Project of Technological Innovation of Hubei Province (No. 2018AAA031), the Science and Technology Project of the Department of Transportation of Hubei Province (Nos. 2018–422-1–2, 2022–11-2–8), and the National Key Research and Development Program of China



(No. 2017YFC0806 008) may all wish to express their sincere gratitude for the financial support provided.

Declaration

Conflict of interest We declare that we do not have any commercial or associative interest that represents a conflict of interest in connection with the work submitted.

Open Access This article is licensed under a Creative Commons Attribution 4.0 International License, which permits use, sharing, adaptation, distribution and reproduction in any medium or format, as long as you give appropriate credit to the original author(s) and the source, provide a link to the Creative Commons licence, and indicate if changes were made. The images or other third party material in this article are included in the article's Creative Commons licence, unless indicated otherwise in a credit line to the material. If material is not included in the article's Creative Commons licence and your intended use is not permitted by statutory regulation or exceeds the permitted use, you will need to obtain permission directly from the copyright holder. To view a copy of this licence, visit <http://creativecommons.org/licenses/by/4.0/>.

References

1. Zhang W, Liu X, Huang Y, Tong M (2022) Reliability-based analysis of the flexural strength of concrete beams reinforced with hybrid BFRP and steel rebars. *Arch Civ Mech Eng*. <https://doi.org/10.1007/s43452-022-00493-7>
2. Yang J, Haghani R, Blanksvärd T, Lundgren K (2021) Experimental study of FRP-strengthened concrete beams with corroded reinforcement. *Constr Build Mater* 301:124076. <https://doi.org/10.1016/j.conbuildmat.2021.124076>
3. Araba AM, Zinkaah OH, Alhawat M, Ashour A (2023) Experimental tests of two span continuous concrete beams reinforced with hybrid GFRP-Steel bars. *Structures* 47:2485–2500. <https://doi.org/10.1016/j.istruc.2022.12.055>
4. Wang X, Liu S, Shi Y, Wu Z, He W (2022) Integrated high-performance concrete beams reinforced with hybrid BFRP and steel bars. *J Struct Eng*. [https://doi.org/10.1061/\(ASCE\)ST.1943-541X.0003207](https://doi.org/10.1061/(ASCE)ST.1943-541X.0003207)
5. Mahroug MEM, Ashour AF, Lam D (2014) Experimental response and code modelling of continuous concrete slabs reinforced with BFRP bars. *Compos Struct* 107:664–674. <https://doi.org/10.1016/j.compstruct.2013.08.029>
6. Wenjun Q, Xiaoliang Z, Haiqun H (2009) Flexural behavior of concrete beams reinforced with hybrid (GFRP and steel) bars. *J Compos Constr*. [https://doi.org/10.1061/\(ASCE\)CC.1943-5614.0000035](https://doi.org/10.1061/(ASCE)CC.1943-5614.0000035)
7. Aiello MA, Ombres L (2002) Structural performances of concrete beams with hybrid (fiber-reinforced polymer-steel) reinforcements. *J Compos Constr* 6(2):133–140. [https://doi.org/10.1061/\(ASCE\)1090-0268\(2002\)6:2\(133\)](https://doi.org/10.1061/(ASCE)1090-0268(2002)6:2(133))
8. YL H, VB R (2003) Flexural behaviour of concrete beams internally reinforced with GFRP rods and steel rebars. *Struct Surv*. <https://doi.org/10.1108/02630800310507159>
9. Lau D, Pam HJ (2010) Experimental study of hybrid FRP reinforced concrete beams. *Eng Struct* 32(12):3857–3865. <https://doi.org/10.1016/j.engstruct.2010.08.028>
10. Ahmed ER, Farid A, Abdullah A (2015) Structural performance and serviceability of concrete beams reinforced with hybrid (GFRP and steel) bars. *Constr Build Mater*. <https://doi.org/10.1016/j.conbuildmat.2015.08.063>
11. Ge W, Zhang J, Cao D, Tu Y (2015) Flexural behaviors of hybrid concrete beams reinforced with BFRP bars and steel bars. *Constr Build Mater* 87:28–37. <https://doi.org/10.1016/j.conbuildmat.2015.03.113>
12. Thamrin R, Zaidir Z, Iwanda D (2022) Ductility estimation for flexural concrete beams longitudinally reinforced with hybrid FRP-steel bars. *Polymers-Basel* 14(5):1017. <https://doi.org/10.3390/polym14051017>
13. Lei P, Wenjun Q, Peng Z, Jiaping X (2015) Design propositions for hybrid FRP-steel reinforced concrete beams. *J Compos Constr*. [https://doi.org/10.1061/\(ASCE\)CC.1943-5614.0000654](https://doi.org/10.1061/(ASCE)CC.1943-5614.0000654)
14. Lu CH, Li H, Xu K, Xuan GY, Abdullah W (2020) Experimental study of flexural behavior and serviceability of hybrid concrete beams reinforced by steel and G/BFRP bars. *IOP conference series. Mater Sci Eng* 770(1):12007. <https://doi.org/10.1088/1757-899X/770/1/012007>
15. Ruan X, Lu C, Xu K, Xuan G, Ni M (2020) Flexural behavior and serviceability of concrete beams hybrid-reinforced with GFRP bars and steel bars. *Compos Struct* 235:111772. <https://doi.org/10.1016/j.compstruct.2019.111772>
16. Qin R, Zhou A, Lau D (2017) Effect of reinforcement ratio on the flexural performance of hybrid FRP reinforced concrete beams. *Compos B Eng* 108:200–209. <https://doi.org/10.1016/j.compositesb.2016.09.054>
17. Abbas H, Abadel A, Almusallam T, Al-Salloum Y (2022) Experimental and analytical study of flexural performance of concrete beams reinforced with hybrid of GFRP and steel rebars. *Eng Fail Anal* 138:106397. <https://doi.org/10.1016/j.engfailanal.2022.106397>
18. Bui LVH, Stitmannaitum B, Ueda T (2018) Ductility of concrete beams reinforced with both fiber-reinforced polymer and steel tension bars. *J Adv Concr Technol* 16(11):531–548. <https://doi.org/10.3151/jact.16.531>
19. Linh VHB, Boonchai S, Tamon U (2017) Mechanical performances of concrete beams with hybrid usage of steel and FRP tension reinforcement. *Comput Concrete*. <https://doi.org/10.12989/cac.2017.20.4.391>
20. Hussein A, Huang H, Okuno Y, Wu Z (2022) Experimental and numerical parametric study on flexural behavior of concrete beams reinforced with hybrid combinations of steel and BFRP bars. *Compos Struct* 302:116230. <https://doi.org/10.1016/j.compstruct.2022.116230>
21. Lu C, Cai Q, Xu K, Sha X, Yan Y (2022) Comparison of flexural behaviors between plain and steel-fiber-reinforced concrete beams with hybrid GFRP and steel bars. *Structures* 43:1–11. <https://doi.org/10.1016/j.istruc.2022.06.037>
22. Si-Larbi A, Ferrier E, Hamelin P (2006) Flexural behaviour of MRBC beams (multi-reinforcing bars concrete



- beams), promoting the use of FRHPC. *Compos Struct* 74(2):163–174. <https://doi.org/10.1016/j.compstruct.2005.04.001>
23. Farid A, Abdul RA (2019) Effect of basalt fibers on the flexural behavior of concrete beams reinforced with BFRP bars. *Compos Struct*. <https://doi.org/10.1016/j.compstruct.2019.02.050>
 24. Haitang Z, Zongze L, Chengcheng W, Shengzhao C, Yunxiao W (2020) Prediction model for the flexural strength of steel fiber reinforced concrete beams with fiber-reinforced polymer bars under repeated loading. *Compos Struct*. <https://doi.org/10.1016/j.compstruct.2020.112609>
 25. Qin Y, Zhang X, Chai J, Xu Z, Li S (2019) Experimental study of compressive behavior of polypropylene-fiber-reinforced and polypropylene-fiber-fabric-reinforced concrete. *Constr Build Mater* 194:216–225. <https://doi.org/10.1016/j.conbuildmat.2018.11.042>
 26. Wang D, Ju Y, Shen H, Xu L (2019) Mechanical properties of high performance concrete reinforced with basalt fiber and polypropylene fiber. *Constr Build Mater* 197:464–473. <https://doi.org/10.1016/j.conbuildmat.2018.11.181>
 27. China MOHA. GB/T 50081–2019. Standard for test methods of concrete physical and mechanical properties. Peking: China Architecture & Building Press, (2019). (In Chinese)
 28. China MOHA. JG/T 248–2009. Apparatus for concrete slump test. Peking: China Architecture & Building Press, (2009). (In Chinese)
 29. China MOHA. GB/T 50080–2016. Standard for test method of performance on ordinary fresh concrete. Peking: China Architecture & Building Press, (2016). (In Chinese)
 30. Standardization CAFE. CECS13: 2009. Standard test methods for fiber reinforced concrete. China Planning Press, (2010) pp. 54–59. (In Chinese)
 31. China MOHA. JGJ/T 221–2010. Technical specification for application of fiber reinforced concrete. Peking: China Architecture & Building Press, (2010). (In Chinese)
 32. ACI 440.1R-15. Guide for the Design and-Construction of Structural Concrete Reinforced with Fiber-Reinforced Polymer (FRP) Bars. American Concrete Institute, Farmington Hills, MI, USA (2015)
 33. COMITE EURO-INTERNATIONAL DB. CEB-FIP Model Code 1990. Thomas Telford, London, (1991)
 34. ACI 440.1R-06. Guide for the design and construction of structural concrete reinforced with FRP bars. American Concrete Institute, Farmington Hills, MI, USA, (2006)
 35. China MOHA. GB/T 50152–2012. Standard for test method of concrete structures. Peking: China Architecture & Building Press, (2012). (In Chinese)
 36. CSA-S806–12. Design and construction of building components with fibre-reinforced polymers. Ontario (Canada): Canadian Standards Association; (2012)
 37. GB50010–2010. Code for design of concrete structures. Beijing: China Building Industry Press, (2010) (In Chinese)
 38. Peter HB, Shawn PG (2011) Equivalent moment of inertia based on integration of curvature. *J Compos Constr*. [https://doi.org/10.1061/\(ASCE\)CC.1943-5614.0000164](https://doi.org/10.1061/(ASCE)CC.1943-5614.0000164)
 39. Yoon YS, Yang JM, Min KH, Shin HO (2011) Flexural strength and deflection characteristics of high-strength concrete beams with hybrid FRP and steel bar reinforcement. *American Concrete Institute, ACI Spec Publ* 1:57–77
 40. Peter HB (2005) Reevaluation of deflection prediction for concrete beams reinforced with steel and fiber reinforced polymer bars. *J Struct Eng*. [https://doi.org/10.1061/\(ASCE\)0733-9445\(2005\)131:5\(752\)](https://doi.org/10.1061/(ASCE)0733-9445(2005)131:5(752))
 41. El Refai A, Abed F, Al-Rahmani A (2015) Structural performance and serviceability of concrete beams reinforced with hybrid (GFRP and steel) bars. *Constr Build Mater* 96:518–529. <https://doi.org/10.1016/j.conbuildmat.2015.08.063>
 42. Canadian highway bridge design code: CSA-S6–10. Mississauga: Canadian Standards Association 2010.
 43. Jaeger L, Mufti A, Tadros G (1997) The concept of the overall performance factor in rectangular-section reinforced concrete members. *Compos Struct* 2:551–559
 44. Naaman A, Jeong S (1995) Structural ductility of concrete beams prestressed with FRP tendons, non-metallic (FRP) reinforcement for concrete structures. *Proceedings of the Second International RILEM Symposium (FRPRCS-2)*, E & FN Spon, London
 45. Yang J, Fang Z (2015) Ductility and deformability of RPC beams prestressed with CFRP tendons. *J Hunan Univ (Natural Sciences)* 42(03):14–22 ((In Chinese))

Publisher's Note Springer Nature remains neutral with regard to jurisdictional claims in published maps and institutional affiliations.

